Dual-Polarized Highly Folded Bowtie Antenna With Slotted Self-Grounded Structure for Sub-6 GHz 5G Applications

Alibakhshikenari, M., Virdee, B. S., See, C. H., Shukla, P., Moghaddam, S. M., Zaman, A. U., Shafqaat, S., Akinsolu, M. O., Liu, B., Yang, J., Abd-Alhameed, R., Falcone, F. and Limiti, E.

Communication

Dual-Polarized Highly Folded Bowtie Antenna With Slotted Self-Grounded Structure for Sub-6 GHz 5G Applications

Mohammad Alibakhshikenari, Bal S. Virdee, Chan Hwang See, Pancham Shukla, Sadegh Mansouri Moghaddam, Ashraf Uz Zaman, Samia Shafqaat, Mobayode O. Akinsolu, Bo Liu, Jian Yang, Raed Abd-Alhameed, Francisco Falcone, and Ernesto Limiti

***Abstract*— In this communication, a novel dual-polarized highly folded self-grounded Bowtie antenna that is excited through I-shaped slots is proposed for applications in sub-6 GHz 5G multiple-input-multiple-output (MIMO) antenna systems. The antenna consists of two pairs of folded radiation petals whose base is embedded in a double layer of FR-4 substrate with a common ground-plane which is sandwiched between the two substrate layers. The ground-plane is defected with two I-shaped slots located under the radiation elements. Each pair of radiation elements are excited through a microstrip line on the top layer with RF signal that is 180° out of phase with respect to each other. The RF signal is coupled to the pair of feedlines on the top layer through the I-shaped slots from the two microstrip feedlines on the underside of the second substrate. The proposed feed mechanism gets rid of the otherwise bulky balun. The Bowtie antenna is a compact solution with dimensions of 32 × 32 × 33.8 mm^3. Measured results have verified that the antenna operates over a frequency range of 3.1–5 GHz and exhibits an average gain and antenna efficiency in the vertical and horizontal polarizations of 7.5 dBi and 82.6%, respectively.**

***Index Terms*— 5G applications, bowtie antenna, dual-polarized, I-shaped slot, multiple-input-multiple-output (MIMO), slotted self-grounded structure, sub-6 GHz.**

Manuscript received May 18, 2021; revised September 3, 2021; accepted September 21, 2021. Date of publication October 14, 2021; date of current version April 7, 2022. This project has received funding in part by the Universidad Carlos III de Madrid and the European Union's Horizon 2020 Research and Innovation Programme under the Marie Sklodowska-Curie Grant 801538, in part by the Ministerio de Ciencia, Innovación y Universidades, Gobierno de Spain (MCIU/AEI/FEDER, UE) under Grant RTI2018-095499-B-C31, in part by the Innovation Program under Grant H2020-MSCA-ITN-2016 SECRET-722424, and in part by the U.K. Engineering and Physical Sciences Research Council (EPSRC) under Grant EP/E022936/1. *(Corresponding author: Mohammad Alibakhshikenari.)*

Mohammad Alibakhshikenari is with the Department of Signal Theory and Communications, Universidad Carlos III de Madrid, 28911 Leganés, Madrid, Spain (e-mail: mohammad.alibakhshikenari@uc3m.es).

Bal S. Virdee and Pancham Shukla are with the Center for Communications Technology, School of Computing and Digital Media, London Metropolitan University, London N7 8DB, U.K.

Chan Hwang See is with the School of Engineering and the Built Environment, Edinburgh Napier University, Edinburgh EH10 5DT, U.K.

Sadegh Mansouri Moghaddam, Ashraf Uz Zaman, Samia Shafqaat, and Jian Yang are with the Department of Electrical Engineering, Chalmers University of Technology, 412 96 Gothenburg, Sweden.

Mobayode O. Akinsolu is with the Faculty of Arts, Science and Technology, Wrexham Glyndŵr University, Wrexham LL11 2AW, U.K.

Bo Liu is with the James Watt School of Engineering, University of Glasgow, Glasgow G12 8QQ, U.K., and also with the School of Electrical, Electronic, and System Engineering, University of Birmingham, Birmingham B15 2TT, U.K.

Raed Abd-Alhameed is with the Faculty of Engineering and Informatics, University of Bradford, Bradford BD7 1DP, U.K.

Francisco Falcone is with the Department of Electrical, Electronic and Communication Engineering and the Institute of Smart Cities, Public University of Navarre, 31006 Pamplona, Spain.

Ernesto Limiti is with the Department of Electronic Engineering, University of Rome "Tor Vergata," 00133 Rome, Italy.

Color versions of one or more figures in this communication are available at https://doi.org/10.1109/TAP.2021.3118784.

Digital Object Identifier 10.1109/TAP.2021.3118784

I. Introduction

The proliferation of wireless technologies and the Internet of Things (IoT) has necessitated the development of next generation of technologies, such as 5G, that provide greater channel capacity and significantly higher data transmission rate compared with 4G/LTE [1]. Moreover, this technology acceleration has driven the hardware to be more compact, easier to integrate, and more economic while offering smarter and more multifunctional characteristics. This has spawned the need for wideband antennas to enable high data throughput [2]. Hence, a lot of effort has been invested over the past several years in developing wideband antennas that meet the requirements of 5G systems and support other multiband and multistandard wireless systems.

Wideband antennas have been investigated extensively, including dual-band antennas [3], multiple-input-multiple-output (MIMO) antennas [4], and phased arrays [5], [6]. In addition, it has been shown that bandwidth improvement can be achieved by using various techniques, such as balun integration [7], coupled resonant structures [8], slot antennas [9], proximity coupled planar arrays [10], air-filled cavities [11], and corporate stacked microstrips [12]. The antenna gain has been enhanced with double-sided Bowtie parasitics [13], lenses [14], and metal directors [15]. Among the numerous types of wideband antennas, the self-grounded Bowtie antenna has the benefit of structural simplicity and compactness [16], [17]. However, wideband antennas are normally excited using various wideband baluns [18] which are often quite large and challenging to implement in a limited space.

In this communication, we present the design and implementation of a novel dual-polarized Bowtie antenna that has a small form factor. The proposed antenna is self-grounded with a novel feed mechanism that has the benefit of reducing the overall size of the antenna as well as manufacturing costs. The antenna is intended for applications in sub-6 GHz 5G Massive MIMO wireless communications systems.

Although the structure of the proposed antenna appears relatively simple, its geometry is defined by 39 parameters, which makes the optimization of antenna's performance a big challenge. Hence, an artificial intelligence (AI)-driven optimization approach is necessary to realize the required performance specifications from the antenna, which is an extension of our previous work [19], where only a simple parameter sweeping was utilized. The AI method of optimization applied here is based on the parallel surrogate model-assisted hybrid differential evolution for antennas (PSADEAs) [20], [24]. PSADEA belongs to the SADEA algorithm series [20]–[24] and is applicable for cases with up to 40 optimization parameters. Compared with other popular global optimization methods, e.g., particle swarm optimization and genetic algorithm, PSADEA provides significantly better results at a much faster speed by a factor of 30.

This article is an extension of our previous work [25]–[27]. The novelty of this work includes: 1) realization of a small form factor

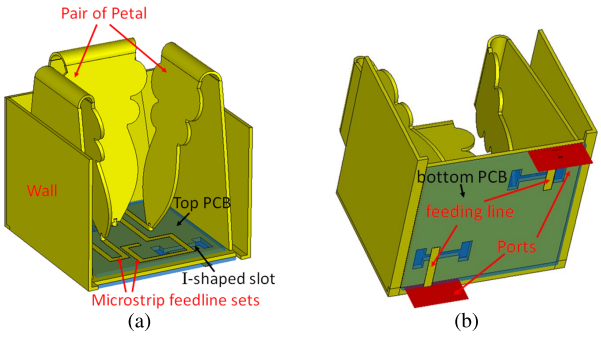

Fig. 1. Geometry of the proposed antenna. Here one petal is hidden for the sake of clarity. (a) Petals and feeding mechanism. (b) Feeding lines below ground plane.

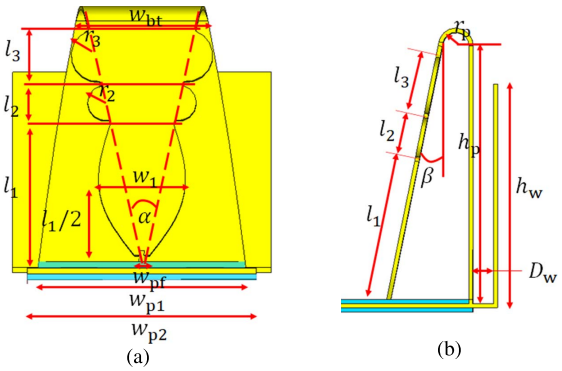

Fig. 2. Geometry of petal and parameters' definitions. (a) Front view. (b) Side view.

dual-polarized Bowtie antenna design; 2) using a highly compact feeding mechanism; 3) reduction of sidelobes by surrounding the radiation petals with a metal wall; and 4) realization of a large beamwidth to enable wide-angle scanning in phased array antennas.

The communication is organized as follows: Section II describes the structure of the proposed dual-polarized Bowtie antenna and the optimization method employed. The simulated and measured results are given in Section III. The work is concluded in Section IV.

II. Highly Folded Self-Grounded Bowtie

The aim of this work was to design a highly compact self-grounded Bowtie antenna for an application in phased array antennas. In this application, the antenna spacing must be limited to $0.5\lambda_0$ to enable wide scanning angles; however, this must be achieved without introducing grating lobes and reduction in the gain and bandwidth that result from strong mutual coupling between adjacent radiators. Moreover, as the beam is steered to a wider angle, there arises an issue that the sidelobe level rises to a nonnegligible level. To circumvent these issues, we have developed a highly folded self-grounded Bowtie antenna illustrated in Fig. 1. The antenna consists of two pairs of radiation petals whose length is about one wavelength, and the pair of petals are arranged orthogonally to realize dual-polarization performance. The parameters defining the structure of the radiation petals are shown in Fig. 2. The three convex sections in the petals provide the required bandwidth of operating between 3.1 and 5.0 GHz. The radiation petals are surrounded with a metal wall to reduce the sidelobes from the antenna.

The antenna structure can be divided into two parts: the radiation petal part and the feeding part. Figs. 2 and 3 show the parameters

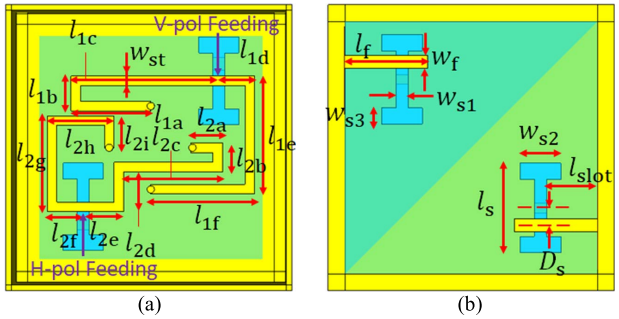

Fig. 3. Geometry of feed mechanism and annotated are the associated parameters. (a) Microstrip feedline set on the top PCB. (b) Microstrip feedline on the underside of the bottom PCB.

TABLE I
Parameters for Defining Radiation Petals and Their Optimized Values

Parameter	Symbol	Optimized value
Width of feeding tip	w_{pf}	2.0 mm
Width of 1st convex	w_1	11.28 mm
Back wall width of petal top	w_{bt}	17.2 mm
Bottom width of petal back wall	w_{p1}	27.1 mm
Width of ground plane	w_{p2}	29.8 mm
Length of 1st convex part	l_1	17.2 mm
Length of 2nd convex part	l_2	5.12 mm
Length of 3rd convex part	l_3	6.98 mm
Radius of circle curve in 2nd convex	r_2	4.39 mm
Radius of circle curve in 3rd convex	r_3	6.51 mm
Extended angle of petal plate	α	26.4°
Petal height	h_p	32.24 mm
Petal top radius	r_p	1.82 mm
Petal tilted angle	β	11.41°
Height of wall	h_w	26.12 mm
Distance between wall and petal	D_w	1.302 mm

that define the geometries of these two parts. The full list of the parameters is given in Tables I and II.

The mechanism to excite the antenna is implemented on a stack of two printed circuit boards (PCBs) of FR-4 substrate that sandwich the common ground-plane. The substrates have a height of 0.768 mm, a dielectric constant (ε_r) of 4.3, and a loss-tangent $\tan(\delta)$ of 0.025. The two microstrip feedlines created on the upper side of the top PCB connect the two pairs of folded petals, as shown in Fig. 3(a). Each of these feedlines is excited by RF signal coupled from the feedlines on the underside of the bottom PCB through the I-shaped slots implemented in the middle ground-plane, as shown in Fig. 3(b). The pair of petals are excited with the RF signal of the same magnitude but 180° out-of-phase by virtue of the connecting microstrip feedline lengths. The proposed feeding mechanism avoids the otherwise need for a bulky balun.

The proposed antenna was modeled in CST Microwave Studio, with a mesh density of 20 cells per wavelength, resulting in total about 400 000 mesh cells for the whole structure. Each full-wave simulation costs on average about 7 min. All simulations and computations reported in this work have been carried out on a workstation with an Intel 8-core i9-9900K 3.6 GHz CPU and a 64 GB RAM, and the time consumptions are wall clock time. Optimizations have been carried out with target goals of: 1) reflection-coefficients below -10 dB; 2) isolation between the two ports greater than 20 dB; 3) antenna gain above 6 dBi; and 4) 3 dB beamwidth larger than $2 \times 40°$ across 3.155 GHz. The objective function used for the

TABLE II
PARAMETERS FOR DEFINING FEEDING STRUCTURE AND THEIR OPTIMIZED VALUES

Parameter	Symbol	Optimized value (mm)
Width of strip line	w_{st}	1.15
1st part length of feeding 1	l_{1a}	9.6
2nd part length of feeding 1	l_{1b}	4.22
3rd part length of feeding 1	l_{1c}	17.76
4th part length of feeding 1	l_{1d}	4.32
5th part length of feeding 1	l_{1e}	14.21
6th part length of feeding 1	l_{1f}	12.48
1st part length of feeding 2	l_{2a}	3.84
2nd part length of feeding 2	l_{2b}	3.46
3rd part length of feeding 2	l_{2c}	11.90
4th part length of feeding 2	l_{2d}	4.80
5th part length of feeding 2	l_{2e}	4.90
6th part length of feeding 2	l_{2f}	4.32
7th part length of feeding 2	l_{2g}	11.52
8th part length of feeding 2	l_{2h}	8.06
9th part length of feeding 2	l_{2i}	3.84
Length of feeding line of input	l_f	9.79
Position of I-shaped slot	l_{slot}	6.0
Width of input feeding line	w_f	1.54
Width of I-shaped slot	w_{s1}	1.44
Length of I-shaped end slot	w_{s2}	4.80
Width of I-shaped end slot	w_{s3}	1.92
Offset of feeding line	D_s	2.02

optimization is stated as follows:

$$\begin{aligned} F_{bowtie} &= w_1 \times \{max([S_{11} - 10\text{ dB}, 0]) + max([S_{22} - 10\text{ dB}, 0]) \\ &\quad + max([S_{12} - 20\text{ dB}, 0]) + max([S_{21} - 20\text{ dB}, 0])\} + w_2 \\ &\quad \times \{min([6\text{ dBi} - G_{real}, 0]) + min([80^\circ - BW_{3\text{ dB}}, 0])\} \end{aligned} \tag{1}$$

where S_{11}, S_{22}, S_{12}, and S_{21} are the in-band S-parameters, G_{real} is the in-band realized gain, and $BW_{3\text{ dB}}$ is the in-band 3 dB beamwidth. w_1 and w_2 are the penalty coefficients set to 1 and 50, respectively, to preferentially ensure that the optimization procedure focuses on satisfying the specifications for G_{real} and $BW_{3\text{ dB}}$ first, by largely penalizing F_{bowtie} if they are violated. Then, meeting the requirements for the S-parameters becomes the primary focus of the optimization procedure as soon as G_{real} and $BW_{3\text{ dB}}$ are satisfied.

CST Microwave Studio was initially employed for the optimization process. However, the results obtained were not satisfactory. This is because the trust region framework of CST optimizer requires the initial design to be good; however, this was not the reason in our case. Using our initial design, CST trust region framework was trapped in a local optimum far from the required specifications. CST global optimization methods, such as genetic algorithm and particle swarm optimization, require hundreds of EM simulations for the size of our structure. Using this method, the calculation cost is too high, and the design efficiency is very low. Therefore, we had to employ an optimization scheme described below. We first optimized the radiation petal part by using genetic algorithm optimizer in CST Microwave Studio. Then, using this preliminarily results we performed an AI-driven optimization approach to optimize the whole antenna structure. This was done using an in-house developed PSADEA algorithm. This was because PSADEA had previously been demonstrated in [20] and [21] to be suitable for complex antenna designs involving challenging geometric constraints and stringent performance requirements, which other standard global optimization methods are not be able to address [28], [29].

PSADEA uses a Gaussian process (GP) to predict new values of geometry parameters based on previous evaluations [30]. PSADEA models a parameter $y(x)$ as a Gaussian distributed stochastic variable with mean μ and variance σ^2. It uses a Gaussian correlation function to describe the correlation between two variables:

$$Corr\left(x_i, x_j\right) = \exp\left(-\sum_{l=1}^{d} \theta_l \left|x_i^l - x_j^l\right|^{p_l}\right), \quad \theta_l > 0,\ 1 \le p_l \le 2 \tag{2}$$

where d represents the dimension of x and θ_l the correlation parameter which determines how fast the correlation decreases when x_i moves in the l-direction. The function p_l determines the degree of smoothness with respect to x^l. To determine the parameters θ_l and p_l, the likelihood function $y = y^i$ at $x = x^i (i = 1, \ldots, n)$ is maximized. The function value $y(x^*)$ at a new point x^* is predicted using

$$\check{y}\left(x^*\right) = \check{\mu} + r^T R^{-1}\left(y - I\check{\mu}\right) \tag{3}$$

where

$$R_{i,j} = Corr\left(x_i, x_j\right), \quad i, j = 1, 2, \ldots, n \tag{4}$$

$$r = \left[Corr\left(x^*, x_1\right), Corr\left(x^*, x_2\right), \ldots, Corr\left(x^*, x_n\right)\right] \tag{5}$$

$$\hat{\mu} = \left(I^T R^{-1} I\right)^{-1} I^T R^{-1} y. \tag{6}$$

The mean square error value of the prediction uncertainty is

$$\hat{s}^2\left(x^*\right) = \hat{\sigma}^2\left[I - r^T R^{-1} r + \left(1 - r^T R^{-1} r\right)^2 \left(r^T R^{-1} I\right)^{-1}\right] \tag{7}$$

where

$$\hat{\sigma}^2 = \left(y - I\hat{\mu}\right)^T R^{-1}\left(y - I\hat{\mu}\right) n^{-1}. \tag{8}$$

Several prescreening methods can be used to evaluate the quality of a given design with respect to the predicted value in (3) and the prediction uncertainty in (7). In PSADEA, the lower confidence bound (LCB) method [31] is used. Given the predictive distribution $N(\hat{y}(x), \hat{s}(x))$ for $y(x)$, an LCB prescreening of $y(x)$ can be defined as:

$$y_{lcb}(x) = \hat{y}(x) - \omega\hat{s}(x), \quad \omega \in [0, 3] \tag{9}$$

where ω is a constant, which is often set to 2 to balance the exploration and exploitation ability [30]. The flow diagram for PSADEA implementation is shown in Fig. 4. More details about how PSADEA works can be found in [20] and [21]. The final optimized parameter values are given in Tables I and II.

III. SIMULATION AND MEASUREMENT RESULTS

Fig. 5 shows the fabricated prototype of the design of the dual-polarized Bowtie antenna. It has dimensions of $32 \times 32 \times 33.8$ mm^3. The figure shows different views of the antenna before and after assembling. Fig. 6 shows the simulated and measured S-parameters of the proposed antenna. The vertically polarized (V-pol) excitation corresponds to the V-pol feedline, and the horizontally polarized (H-pol) excitation is due to the H-pol feedline on the top PCB, as shown in Fig. 3(a). It is observed that the antenna exhibits an excellent impedance matching performance for both V-pol (S_{11}) and H-pol (S_{22}) cases. The simulated and measured $|S_{11}|$ and $|S_{22}|$ are below -10 dB over 3.08–4.74 and 3.29–5.0 GHz, which correspond to fractional bandwidths (FBWs) of 42% and 41%, respectively. The difference between the simulated and measured

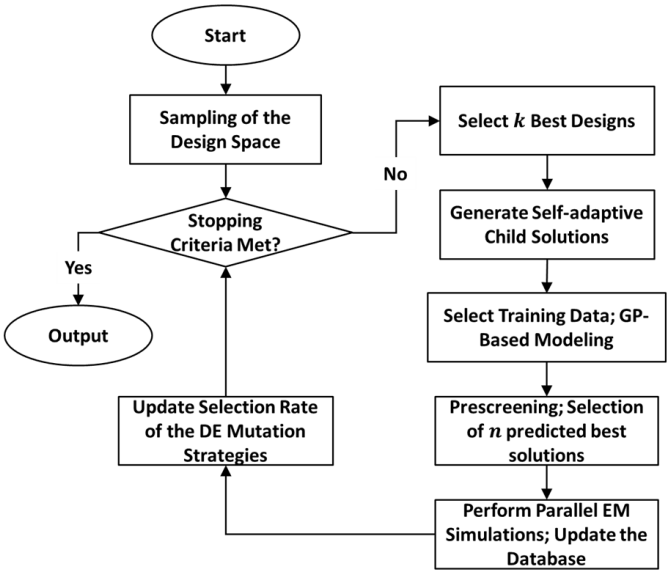

Fig. 4. PSADEA flow diagram.

Fig. 5. Fabricated prototype of the proposed dual-polarized bowtie antenna.

$|S_{11}|$ and $|S_{22}|$ is marginal. The discrepancy in the S-parameters of the two polarizations is due to the asymmetry of the feedlines as well as manufacturing and assembly tolerance. The measured isolation between the ports of different polarizations is larger than 28 dB, which agrees well with the simulation results. These results show the optimization goal of the simulation agrees well with the measurements.

The simulated and measured gain and radiation efficiency of the proposed antenna are shown in Fig. 7. The antenna gain was measured by using the substitution method with a calibrated reference antenna. The discrepancy between the simulation and measured results is attributed to ohmic and the mismatching losses. The measured antenna gain varies between 7.4 and 7.8 dBi for vertical

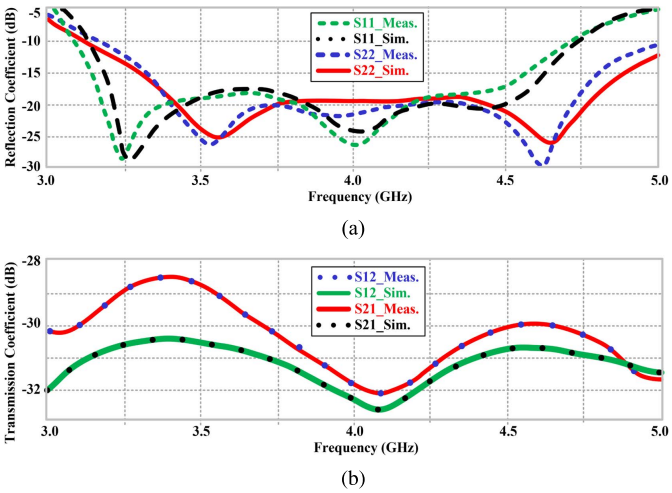

Fig. 6. S-parameters of V-pol and H-pol ports of the proposed antenna. (a) Reflection coefficients (V-pol S_{11} and H-pol S_{22}). (b) Transmission coefficients between V-pol and H-pol ports.

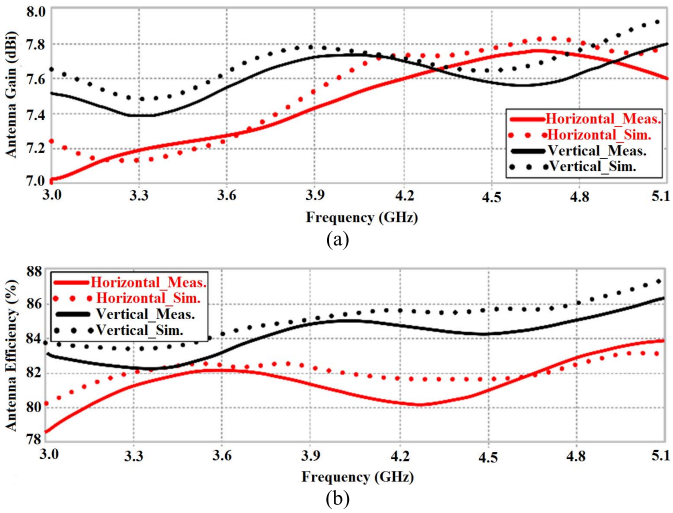

Fig. 7. Radiation performance of the proposed antenna over the operation band. (a) Antenna gain. (b) Antenna efficiency.

polarization, and between 7 and 7.78 dBi for horizontal polarization over 3–5.1 GHz. These results satisfy the optimization goals.

Measurements show that the radiation efficiency of the antenna varies between 82% and 86.2% in vertical polarization, and between 78.8% and 83.9% in horizontal polarization over 3–5.1 GHz. The average discrepancy in the measured results between the vertical and horizontal polarization of the gain and radiation efficiency is 0.3 dBi and 3.7%, respectively. The reason that the antenna gain for H-pol is a bit lower than that for V-pol is that the feedline for H-pol is longer and with more bends, as shown in Fig. 3(a). However, there is good coherence between the simulated and the experimental results.

The self-grounded Bowtie antenna is a quasi-BOR_1 antenna and the radiation performance can be described fully by the 45°-plane co- and cross-polar radiation patterns [25]–[27]. Simulated and experimental radiation patterns of the proposed antenna in 45°-plane at three frequency points are shown in Fig. 8. The antenna gain is stable over the frequency band while the beamwidth is broader (3 dB beamwidth is about $2 \times 60°$). This is quite a unique characteristic, which is very good for large scan phased array antennas. The simulated and experimental results are in reasonable agreement. These

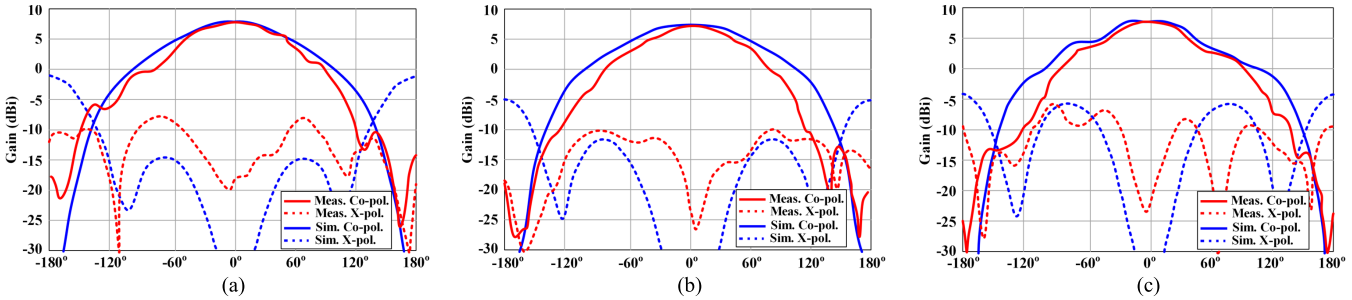

Fig. 8. Simulated and measured radiation patterns of vertical polarization in $\varphi = 45°$ plane. (a) 3 GHz. (b) 4 GHz. (c) 5 GHz.

TABLE III
STATE-OF-THE-ART COMPARISON

characteristics	[25]	[26]	[27]	this work
Feed mechanism	balun	two hybrids	balun	slots
Bandwidth (GHz)	2.0-5.5	1.3-3.0	1.6-2.7	3.1-5.0
Average gain (dBi)	7	5	6	7.5
Average efficiency	89%	76% (sim)	-	82.6%
Polarization	single	dual	dual	dual
Footprint (λ_0^2)	1.5×1.7	0.8×0.8	0.7×0.7	0.4×0.4
Complexity	middle	complicated	middle	simple

results demonstrate the proposed antenna is viable for applications in 5G sub-6 GHz wireless systems.

Table III gives a comparison between the proposed highly folded self-grounded antenna and the previously published work on Bowtie antennas in terms of feed approach, bandwidth, antenna gain, efficiency, polarization, footprint size, and complexity. Although the self-grounded Bowtie antenna was first introduced in [25] it was a single-polarized antenna that used a PCB microstrip balun to excite the radiation petals. The balun was used to transform a 50 Ω impedance microstrip line to a 150 Ω twin-line whose length was too large to implement dual polarization. In [26], a self-grounded dual-polarized Bowtie antenna was designed and excited through four ports connected to two 180° hybrids used as baluns. In [27], the dual-polarized self-grounded Bowtie antenna was realized by using a complex balun circuit to feed its dual-polarized radiation petal pairs. The balun is designed based on the composite right–left handed transmission-line concept.

In this communication, we have replaced the complicated balun designs with a simple feed structure that couples electromagnetic energy from the input feedlines on the underside of the bottom substrate to the feedlines connected to the radiation elements on the top side of the top substrate. The electromagnetic energy is coupled through a pair of I-shaped slots implemented on the common ground-plane which is sandwiched between the two substrates. With the proposed feed mechanism: 1) dual polarization of a Bowtie antenna can be realized in a small form factor and 2) use of a balun is avoided. The proposed technique can be applied to other antennas that require differential feed.

IV. CONCLUSION

A novel configuration of a dual-polarized dual-port Bowtie antenna is shown to exhibit excellent radiation characteristics over a wideband from 3.1 to 5 GHz, making it suitable for sub-6 GHz 5G wireless communications systems. The design has been verified by simulations and measurements. Essentially, the antenna comprises four-folded radiation petals embedded on two layers of FR-4 substrate. Each pair of vertical and horizontal petals can be excited separately to create any dual polarization, such as dual linear polarization or dual circular polarization. The new feeding structure is compact and replaces the otherwise bulky balun used in prior designs with no compromise in performance. The isolation between the two excitation ports is greater than 28 dB. The antenna has an average gain of 7.5 dBi and average radiation efficiency of 82.6% for vertical and horizontal polarizations. The antenna's dimensions are $32 \times 32 \times 33.8$ mm^3. The proposed antenna has a small form factor, is straightforward to integrate with RF electronics, and is relatively easy of manufacture.

REFERENCES

[1] J. G. Andrews *et al.*, "What will 5G be?" *IEEE J. Sel. Areas Commun.*, vol. 32, no. 6, pp. 1065–1082, Jun. 2014.
[2] J. Zhang, X. Ge, Q. Li, M. Guizani, and Y. Zhang, "5G millimeter-wave antenna array: Design and challenges," *IEEE Wireless Commun.*, vol. 24, no. 2, pp. 106–112, Apr. 2017.
[3] Y. Kim and W. Hong, "Co-existence issues concerning 4G and mmWave 5G antennas for mobile terminals," in *Proc. 6th Asia–Pacific Conf. Antennas Propag. (APCAP)*, Xi'an, China, Oct. 2017, pp. 16–19.
[4] O. M. Haraz, "Broadband and 28/38-GHz dual-band printed monopole/elliptical slot ring antennas for the future 5G cellular communications," *J. Infr., Millim., THz Waves*, vol. 37, no. 4, pp. 308–317, Apr. 2016.
[5] Y. Li, C. Wang, H. Yuan, N. Liu, H. Zhao, and X. Li, "A 5G MIMO antenna manufactured by 3-D printing method," *IEEE Antennas Wireless Propag. Lett.*, vol. 16, pp. 657–660, 2017.
[6] I. Syrytsin, S. Zhang, and G. F. Pedersen, "User impact on phased and switch diversity arrays in 5G mobile terminals," *IEEE Access*, vol. 6, pp. 1616–1623, 2018.
[7] S. X. Ta, H. Choo, and I. Park, "Broadband printed-dipole antenna and its arrays for 5G applications," *IEEE Antennas Wireless Propag. Lett.*, vol. 16, pp. 2183–2186, 2017.
[8] C.-X. Mao, S. Gao, and Y. Wang, "Broadband high-gain beam-scanning antenna array for millimeter-wave applications," *IEEE Trans. Antennas Propag.*, vol. 65, no. 9, pp. 4864–4868, Sep. 2017.
[9] A. Dadgarpour, M. S. Sorkherizi, and A. A. Kishk, "Wideband low-loss magnetoelectric dipole antenna for 5G wireless network with gain enhancement using meta lens and gap waveguide technology feeding," *IEEE Trans. Antennas Propag.*, vol. 64, no. 12, pp. 5094–5101, Dec. 2016.
[10] H. A. Diawuo and Y. Jung, "Broadband proximity-coupled microstrip planar antenna array for 5G cellular applications," *IEEE Antennas Wireless Propag. Lett.*, vol. 17, no. 7, pp. 1286–1290, Jul. 2018.
[11] X. Li, J. Xiao, Z. Qi, and H. Zhu, "Broadband and high-gain SIW-fed antenna array for 5G applications," *IEEE Access*, vol. 6, pp. 56282–56289, 2018.
[12] J. Xu, W. Hong, Z. H. Jiang, and H. Zhang, "Wideband, low-profile patch array antenna with corporate stacked microstrip and substrate integrated waveguide feeding structure," *IEEE Trans. Antennas Propag.*, vol. 67, no. 2, pp. 1368–1373, Feb. 2019.
[13] Q.-X. Chu, X.-R. Li, and M. Ye, "High-gain printed log-periodic dipole array antenna with parasitic cell for 5G communication," *IEEE Trans. Antennas Propag.*, vol. 65, no. 12, pp. 6338–6344, Dec. 2017.
[14] E. Kim, S. T. Ko, Y. J. Lee, and J. Oh, "Millimeter-wave tiny lens antenna employing U-shaped filter arrays for 5G," *IEEE Antennas Wireless Propag. Lett.*, vol. 17, no. 5, pp. 845–848, May 2018.

[15] H. Liu, W. Yang, A. Zhang, S. Zhu, Z. Wang, and T. Huang, "A miniaturized gain-enhanced antipodal Vivaldi antenna and its array for 5G communication applications," *IEEE Access*, vol. 6, pp. 76282–76288, 2018.

[16] M. Rumney, R. Pirkl, M. H. Landmann, and D. A. Sanchez-Hernandez, "MIMO over-the-air research, development, and testing," *Int. J. Antennas Propag.*, vol. 2012, Sep. 2012, Art. no. 467695.

[17] A. Khatun *et al.*, "Experimental verification of a plane-wave field synthesis technique for MIMO OTA antenna testing," *IEEE Trans. Antennas Propag.*, vol. 64, no. 7, pp. 3141–3150, Jul. 2016.

[18] S. Lim and H. Ling, "Design of electrically small Yagi antenna," *Electron. Lett.*, vol. 43, no. 5, pp. 256–257, Mar. 2007.

[19] M. Alibakhshikenari, S. M. Moghaddam, A. Uz Zaman, J. Yang, B. S. Virdee, and E. Limiti, "Wideband sub-6 GHz self-grounded bow-tie antenna with new feeding mechanism for 5G communication systems," in *Proc. 13th Eur. Conf. Antennas Propag. (EuCAP)*, Krakow, Poland, Mar./Apr. 2019, pp. 1–4.

[20] B. Liu, M. O. Akinsolu, N. Ali, and R. Abd-Alhameed, "Efficient global optimisation of microwave antennas based on a parallel surrogate model-assisted evolutionary algorithm," *IET Microw., Antennas Propag.*, vol. 13, no. 2, pp. 149–155, Feb. 2019.

[21] M. O. Akinsolu, B. Liu, V. Grout, P. I. Lazaridis, M. E. Mognaschi, and P. Di Barba, "A parallel surrogate model assisted evolutionary algorithm for electromagnetic design optimization," *IEEE Trans. Emerg. Topics Comput. Intell.*, vol. 3, no. 2, pp. 93–105, Apr. 2019.

[22] B. Liu, H. Aliakbarian, Z. Ma, G. A. E. Vandenbosch, G. Gielen, and P. Excell, "An efficient method for antenna design optimization based on evolutionary computation and machine learning techniques," *IEEE Trans. Antennas Propag.*, vol. 62, no. 1, pp. 7–18, Jan. 2014.

[23] B. Liu, S. Koziel, and N. Ali, "SADEA-II: A generalized method for efficient global optimization of antenna design," *J. Comput. Des. Eng.*, vol. 4, no. 2, pp. 86–97, 2017.

[24] B. Liu *et al.*, "An efficient method for complex antenna design based on a self adaptive surrogate model-assisted optimization technique," *IEEE Trans. Antennas Propag.*, vol. 69, no. 4, pp. 2302–2315, Apr. 2021.

[25] J. Yang and A. Kishk, "A novel low-profile compact directional ultra-wideband antenna: The self-grounded bow-tie antenna," *IEEE Trans. Antennas Propag.*, vol. 60, no. 3, pp. 1214–1220, Mar. 2012.

[26] H. Raza, A. Hussain, J. Yang, and P.-S. Kildal, "Wideband compact 4-port dual polarized self-grounded bowtie antenna," *IEEE Trans. Antennas Propag.*, vol. 62, no. 9, pp. 4468–4473, Sep. 2014.

[27] S. M. Moghaddam, A. A. Glazunov, and J. Yang, "Wideband dual-polarized linear array antenna for random-LOS OTA measurement," *IEEE Trans. Antennas Propag.*, vol. 66, no. 5, pp. 2365–2373, May 2018.

[28] Q. Hua *et al.*, "A novel compact quadruple-band indoor base station antenna for 2G/3G/4G/5G systems," *IEEE Access*, vol. 7, pp. 151350–151358, 2019.

[29] J. Zhang, M. O. Akinsolu, B. Liu, and G. A. E. Vandenbosch, "Automatic AI-driven design of mutual coupling reducing topologies for frequency reconfigurable antenna arrays," *IEEE Trans. Antennas Propag.*, vol. 69, no. 3, pp. 1831–1836, Mar. 2021.

[30] M. T. M. Emmerich, K. C. Giannakoglou, and B. Naujoks, "Single- and multiobjective evolutionary optimisation assisted by Gaussian random field metamodels," *IEEE Trans. Evol. Comput.*, vol. 10, no. 4, pp. 421–439, Aug. 2006.

[31] J. E. Dennis and V. Torczon, "Multidisciplinary design optimisation: State of the art," in *Managing Approximation Models in Optimization*, N. M. Alexandrov and M. Y. Hussaini, Eds. Philadelphia, PA, USA: SIAM, 1997, pp. 330–347.